Cell Death & Differentiation (2020) 27:1765–1781
https://doi.org/10.1038/s41418-019-0460-0

Cell Death & Differentiation

ARTICLE

Corrected: Correction

Macrophage-derived CCL5 facilitates immune escape of colorectal cancer cells via the p65/STAT3-CSN5-PD-L1 pathway

Chao Liu[1,2] · Zhaoying Yao[1,2] · Jianing Wang[3] · Wen Zhang[1,2] · Yan Yang[4] · Yan Zhang[5] · Xinliang Qu[6] · Yubing Zhu[1,2] · Jianjun Zou[1,2] · Sishi Peng[2,7] · Yan Zhao[1,2] · Shuli Zhao[7] · Bangshun He[7] · Qiongyu Mi[7] · Xiuting Liu[8] · Xu Zhang[9,10,11] · Qianming Du[7]

Received: 20 April 2019 / Revised: 5 November 2019 / Accepted: 11 November 2019 / Published online: 4 December 2019

Abstract

Infiltrated macrophages are an important constituent of the tumor microenvironment and play roles in tumor initiation and progression by promoting immune evasion. However, the molecular mechanism by which macrophage-derived cytokines foster immune escape of colorectal cancer (CRC) is unclear. Here, we demonstrated that macrophage infiltration induced by lipopolysaccharide (LPS) or a high-cholesterol diet (HCD) significantly promoted CRC growth. Similarly, LPS and poly (I:C) remarkably increased the volume of CT26 cell allograft tumors. C-C motif chemokine ligand 5 (CCL5), which is secreted by macrophages, inhibited T-cell-mediated killing of HT29 cells and promoted immune escape by stabilizing PD-L1 in vitro and in vivo. Mechanistically, CCL5 resulted in formation of nuclear factor kappa-B p65/STAT3 complexes, which bound to the COP9 signalosome 5 (CSN5) promoter, leading to its upregulation. Moreover, CSN5 modulated the deubiquitination and stability of PD-L1. High expression of CSN5 in CRC was associated with significantly shorter survival. Furthermore, compound-15 was identified as an inhibitor of CSN5, and destabilized PD-L1 to alleviate the tumor burden. Our results suggest that the novel CCL5-p65/STAT3-CSN5-PD-L1 signaling axis is significantly activated by LPS or HCD-driven macrophage infiltration in an animal model of CRC, which likely has therapeutic and prognostic implications for human cancers.

Introduction

Cancer is a complex system in which a variety of cell types interact. Macrophages, which constitute up to 50% of a solid tumor mass, are a major type of tumor-infiltrating immune cell [1]. Macrophages infiltrated in the tumor microenvironment (TME) are reported to have conflicting functions, that is, they positively or negatively impact tumor growth and progression by interacting with the TME [2]. However, a high density of tumor-associated macrophages (TAMs) is generally correlated with a poor prognosis in the majority of human cancers [3, 4]. Therefore, the role of macrophages in colorectal cancer (CRC) progression is somewhat controversial and needs further investigation.

The responses of cytotoxic T lymphocytes are critical for anti-tumor immunity. TAMs suppress the $CD8^+$ T cell response to cancer by directly interacting with T cells or by secreting immunosuppressive factors [5]. TAMs exert an immunosuppressive effect by producing the chemokines CCL17, CCL18, and CCL22, which preferentially recruit non-cytotoxic T cell subsets [6]. CCL5 plays an important role in CRC. For example, the infiltration of $CD8^+$ T cells to primary CRC sites was dramatically increased in $CCL5^{-/-}$ compared to control mice [7]. To date, although much work has focused on the molecular basis of TAM-mediated immune escape of tumors, the mechanism by which TAM-secreted chemokines regulate immunosuppression in CRC is unclear.

Programmed cell death ligand 1 (PD-L1) is expressed on various cell types. Upon binding to programmed cell death

These authors contributed equally: Chao Liu, Zhaoying Yao, Jianing Wang

Edited by J.P. Medema

Supplementary information The online version of this article (https://doi.org/10.1038/s41418-019-0460-0) contains supplementary material, which is available to authorized users.

✉ Qianming Du
duqianming@njmu.edu.cn

✉ Xu Zhang
Jason151X7@stu.cpu.edu.cn

Extended author information available on the last page of the article.

receptor 1 (PD-1), which is typically expressed on activated T cells, an inhibitory activity of cytotoxic T cells was observed. For example, PD-L1 overexpression on cancer cells leads to apoptosis or impaired activity of tumor-infiltrating T cells, resulting in immune escape [8]. Although anti-PD-1/PD-L1 immune checkpoint blockade therapy has shown promise in breast cancer, non-small cell lung cancer, and colon cancer, there are still many cancer patients do not respond to anti-PD-1/PD-L1 immunotherapy. Therefore, a better understanding of the mechanism of tumor escape mediated by PD-L1 is essential for cancer therapy.

Deubiquitinating enzymes (DUBs), which mediate the removal of Ubiquitin (Ub) from Ub-conjugated substrate proteins, are members of the protease superfamily (cysteine- and metallo-proteases) [9]. The COP9 signalosome (CSN) can exhibit metalloprotease activity by the MPN^{+}/JAMM domain of CSN5/JAB1 (referred to as CSN5) [10, 11]. CSN5 has been linked to tumor survival and implicated as a prognostic marker for multiple cancers [12, 13]. Furthermore, CSN5 reportedly deubiquitinates IκBa, Snail, and PD-L1, promoting tumor progression and migration [14, 15]. Collectively, these findings reveal a close link between CSN5 and carcinoma.

We reported previously that a high-cholesterol diet (HCD) induces macrophage infiltration [16]. Furthermore, lipopolysaccharide (LPS), a potent activator of monocytes and macrophages, triggers secretion of cytokines by macrophages [17, 18]. Therefore, macrophage infiltration was induced by a HCD and LPS, and significantly promoted CRC growth. We investigated the effect and molecular mechanism of TAM-derived cytokines/chemokines on tumor immune escape in mice with AOM-induced CRC. Our findings not only enhance our understanding of macrophage-induced immunosuppression but also provide information that will enable the development of more effective therapies for cancer.

Materials and methods

Cell lines, reagents, and chemicals

HCT-8, HCT-116, SW620, SW480, DLD-1, CaCo-2, CT26, and HT-29 cell lines were purchased from American Type Culture Collection (Manassas, VA, USA) and were independently validated by short tandem repeat DNA fingerprinting at Guangzhou Cellcook biotech Co., Ltd (Guangdong, China). These cells were cultured in Dulbecco's modified Eagle's medium (DMEM), McCoy's 5a medium or RPMI-1640 medium supplemented with 10% fetal bovine serum (Gibco, Vienna, Austria). The cell lines were used for experiments within ten passages after thawing. All cell lines were free of mycoplasma contamination. The antibodies used in our study for western blotting, immunofluorescence and CO-IP were listed in Supplementary Table S1. U0126, PD98059, Bay 11-7082, SB203580, and LY294002 were bought from Cell Signaling Technology (Beverly, MA, United States). Rapamycin, parthenolide, niclosamide, nutlin, MG-132, clodronate, azoxymethane (AOM), LPS, actinomycin D (Act D), cycloheximide (CHX) and cholesterol were purchased from Sigma-Aldrich (St. Louis, MO, USA).

Mice and tumor models

Male C57BL/6 mice, $Rag^{-/-}$ mice (6–8 weeks old) were purchased from the Model Animal Research Center of Nanjing University (Nanjing, China), and all procedures performed here were conducted under the Guide for the Care and Use of Laboratory Animals (USA) and approved by the Institutional Animal Care and Use Committee of Nanjing Medical University. All mice were housed in the specific pathogen-free conditions. Thirty male mice were randomly assigned to AOM, AOM/LPS, and AOM/HCD group ($n = 10$). Randomization was conducted by the methods described as follows: 30 mice, named as 1, 2, 3, etc., were listed in the first column of Execl, and 30 random numbers, corresponded to the animal numbers, were generated in the second column using the function of RAND(), which were sorted in descending order. The ten ones of the thirty mice were assigned to AOM group, and the ten twos to the AOM/LPS group, etc. Animal model of AOM and AOM/HCD was performed as our previous study described [16]. Briefly, mice in each group were intraperitoneally injected with AOM (15 mg/kg body weight) weekly for 4 weeks, subsequently, mice in AOM/HCD group were fed with a normal diet containing 2% cholesterol for 60 days. For the establishment of AOM/LPS model, mice were intraperitoneally injected with LPS (10 μg) every 10 days for 60 days after the last AOM treatment. For treatment with antibodies, 50 μg of CCL5 antibody (R&D systems, Minneapolis, USA) or control rat IgG (Bioxcell, West Lebanon, NH, USA) was injected intraperitoneally every 5 days for 60 days after the last AOM treatment. C-15 was administered at a dose of 20 mg/kg for 88 days. For macrophages depletion, mice were injected with 100 μL of clodronate liposome (ClodronateLiposomes.com, The Netherlands) or PBS liposome (ClodronateLiposomes.com) intraperitoneally every 5 days for 60 days after the last AOM treatment. For the measurement of CCL5 levels, blood was obtained from the post-orbital vein complex after clodronate challenge and CCL5 levels in serum and colon were determined by ELISA. For exogenous administration of CCL5, C57BL/6 mice were injected intraperitoneally every 5 days for 60 days after the last AOM treatment with 2 μg of recombinant murine RANTES (CCL5) (PeproTech,

London, UK) in 100 µL PBS or PBS for control. For PD-1 checkpoint blockade, mice were given 200 µg of anti-PD-1 antibody (Bioxell, West Lebanon, New Hampshire, USA) diluted to 200 µl with PBS every 5 days for 60 days by intraperitoneal (i.p.) injections. Mice were euthanized at day 88 unless otherwise stated, and the colons were removed for further study. Blinding was involved in histological studies. Sample sizes were selected based on expected effect size. Sample sizes (n) indicated in figure legends refer to the number of animal.

To establish the allograft model, 1×10^7 CT26 cells (transfected with/without the indicated plasmid) were injected subcutaneously into male 6–8-week-old C57BL/6 mice, and mice were intraperitoneally administrated with or without 10 µg of LPS or poly (I:C) in PBS or PBS alone every 6 days for 30 days after inoculation. C-15 was administered at a dose of 20 mg/kg for 30 days. For $CD8^+$ T cell depletion, mice were intraperitoneally injected with 250 µg anti-CD8 antibody before C-15 treatment. Tumors were evaluated every 3 days, and the volume was calculated by the following formula: tumor volume $= 0.5 \times$ length $\times$ width^2. The animals were sacrificed at day 30 and the tumors were removed for further study.

Western blot and immunocytochemistry

Colon cancer cells subjected to different treatment were first lysed using a lysis buffer. After separation by SDS-PAGE, the protein was transferred to a PVDF membrane, and blocked with milk in TBST and then incubated with primary antibodies against PD-L1 (Abcam), p-p65 (Abcam), p65 (Cell Signaling Technology), p-STAT3 (Cell Signaling Technology), STAT3 (Cell Signaling Technology), and CSN5 (Abcam). HRP-conjugated goat anti-mouse IgG was used as secondary antibodies. All the experiments were repeated at least three times.

For immunocytochemistry, cells grown on coverslips were fixed with 4% paraformaldehyde for 15 min and permeabilised with 0.1% Triton X-100 for 10 min. Cells were then incubated with 3% bovine serum albumin in PBS for 30 min to block the nonspecific binding sites. Cells were incubated overnight with anti-CSN5 and anti-PD-L1 primary antibody. After washing, cells were stained with a matching Alexa Fluor 488- or 594-conjugated secondary antibody (Life Technologies) at RT for 1 h, followed by DAPI staining (Invitrogen). Signals were visualized using a Confocal Laser Scanning Microscope.

Flow cytometry, immunofluorescence, and coimmunoprecipitation (CO-IP)

Tumor tissues of colon were processed to a single cell suspension as described previously [19]. Cells were counted prior to staining with CD11b-APC/Cy7, F4/80-APC, CD8-APC/Cy7, interferon (IFN)-γ-Pacific Blue, CD3-PerCP, CD25-PE/APC, CD4-PE/Cy5, and FoxP3-PE/Cy7 antibodies. All antibodies were bought from BioLegend (San Diego, CA, USA). Stained samples were analyzed on a FACS Canto II cytometer (BD Biosciences, San Jose, CA, USA).

For Immunofluorescence, colonic tumor sections of 5-µm thickness were blocked with 10% goat serum for 30 min at RT and then incubated with Granzyme B (Abcam), CD8 (Abcam), F4/80 (Abcam), αSMA (Abcam), and PD-L1 (Abcam) primary antibodies overnight at 4 °C. Donkey anti-goat Alexa 488 and donkey anti-rat Alexa 594 were used as secondary antibodies for 1 h at RT. The nuclear was stained with DAPI. Images were viewed by confocal microscope.

For coimmunoprecipitation assay, HT-29 cells were transfected with shRNA for p65 or STAT3 and then stimulated with CCL5. Cells were lysed in (10 mM HEPES (PH8.0), 1.5 mM $MgCl_2$, 10 mM KCl, and 0.5% Nonidet P-40). Immunoprecipitation was carried out using 1 µg of anti-p65 (Cell signaling Technology) antibody or anti-STAT3 antibody (Cell signaling Technology). Western blot was performed as described above.

Preparation of macrophage-conditioned medium (MP)

Macrophage-conditioned medium containing CCL5 was prepared as described previously [20]. Briefly, primary blood monocytes or primary human macrophages were plated in flasks, and cultured in RPMI 1640 medium containing 10% heat-inactivated human serum. Two hours after incubation, adherent cells were isolated and resuspended in medium supplemented with 40 ng/ml human macrophage colony-stimulating factor (MCSF). Cells were cultured in the presence of MCSF for 7 days and then the medium was changed into fresh medium without MCSF on day 7. The cells were cultured for 24 h and the macrophages were finally exposed to 100 ng/ml LPS or 20 µg/ml poly (I:C) for another 12 h. The culture medium was collected, centrifuged, and stored in aliquots at a temperature of −80 °C, and then the macrophage-conditioned medium was obtained.

PD-L1/ PD-1 binding assay and T cell-mediated HT29 cells killing assay

For the measurement of PD-1 and PD-L1 interaction, HT29 cells were seeded into 96-well plates, incubated with recombinant human PD-1 Fc protein and antihuman Alexa Fluor 488 conjugate. The nuclear was stained with DAPI. PD-1 binding affinity of HT29 cells or other colon cancer cell lines treated with MP alone or in combination with the indicated antibodies was analyzed every 2 h.

T cell-mediated tumor cell killing assay was performed as described previously with slight modifications [14] and determined by CCK8 assay or colony formation assay. Briefly, T cells were pre-activated with CD3 antibody (100 ng/ml) and IL-2 (10 ng/ml). Then the HT29 cells were co-cultured with T cells for 24 h followed by treatment with MP and/or the indicated antibodies. CCK8 solution (10 µl) was added into each well and incubated for 1 h. Cell viability was analyzed by microplate reader at 450 nm. For the colony formation assay, HT29 tumors cells and activated T cells were co-cultured in six-well plates. On the following day, cells were exposed to MP and the indicated antibodies. Cells were grown at 37 °C for 7 days and the surviving HT29 tumor cells were stained by crystal violet. Colonies (50 or more cells) were counted by an inverted microscope.

Lentiviral infection and plasmids transfection

The lentiviral-based short hairpin RNAs (shRNAs) or overexpression plasmids used to silence or over-express the PD-L1, CSN5, p65, and STAT3 gene were purchased from GeneChem Company (Shanghai, China). Puromycin (1 µg/ml, InvivoGen, San Diego, CA, USA) was employed to select the transfected cells 48 h after lentiviral transfection. The targeting sequence of shRNA is listed in Supplementary Table S2.

Quantitative RT-PCR and chromatin immunoprecipitation (ChIP)

Total RNA was purified by the RNeasy Mini Kit (Qiagen, Valencia, CA) and used to synthesize the cDNA according to the manufacturer's instructions. For quantification of mRNA levels, GAPDH level was used as an internal control. Real-time PCR was performed using THUNDERBIRD SYBR qPCR Mix (Toyobo) in a StepOnePlus™ Real-Time PCR instrument (Life Technologies). Statistical analysis was conducted using Graphpad Prism Software. Primer sequences for specific genes are shown in Supplementary Table S3.

ChIP was performed using a ChIP Assay Kit (Cell Signaling Technology). The cells were cultured in media containing 1% formaldehyde for 10 min at room temperature. Thereafter, wash the crossed-linked cells twice, and lyse in SDS buffer. Nuclear extracts were fragmentized to 1 kb by sonication. The harvested supernatants were diluted in ChIP dilution buffer and pre-cleared with proteinA Agarose/Salmon Sperm DNA. Immunoprecipitations were conducted with antibodies against STAT3 (Cell signaling Technology), p65 (Cell signaling Technology), and IgG (control). The immunoprecipitated DNA was amplified by PCR. The primers used for mRNA detection and amplification of the binding site of STAT3 in the promoter region of CSN5 are listed in Supplementary Table S3.

ELISA

Cytokine from macrophages was determined by ELISA 24 h after PBS, LPS, or poly (I:C) challenge as previously described [21] using appropriately diluted culture supernatants or serum. Cytokine levels were measured by specific ELISA kits for murine CCL5 (R&D systems, Minneapolis, USA), IL-1β (Invivogen, San Diego, USA), CXCL3 (abcam, Cambridge, UK), IL-6 (Invivogen, San Diego, USA), IL-8 (Invivogen, San Diego, USA), and TNF-α (Cell signaling Technology, Beverly, United States). The assays were performed according to the manufacturer's directions.

Cell-free assay of PD-L1 deubiquitination

For the in vitro deubiquitination assay, HA-PD-L1 was ubiquitinated in vitro as previous described [22] and separated from free ATP by centrifugation. Ubiquitinated PD-L1 (Ub-PD-L1) was then incubated with recombinant Flag-CSN5 in 30 µl deubiquitination buffer containing Tris-HCl (50 mM, PH 7.4), NaCl (150 mM), DTT (10 mM), and $MgCl_2$ (5 mM). The reaction was carried out at 37 °C for 2 h and stopped by adding 25 µl 2×SDS (final concentration 1%) sample buffer and boiling for 5 min. After immunoprecipitated with anti-HA antibody, PD-L1 was analyzed by western blot with anti-ubiquitin antibody.

Luciferase assay

To confirm the effect of CCL5 on activation of CSN5 promoter, we conducted the dual-luciferase reporter assay. HT29 cells were transfected with the pEZX-COPS5 Luc plasmid (GeneCopoeia) using Lipo2000 (Life Technologies) (CSN5-Luc). PRL-TK (Promega) was used for normalization of transfection efficiency. To investigate the STAT3-binding site of CSN5 promoter, progressive 5′-deletion mutants of the CSN5 promoter were constructed as described previously [23] and transfected into HT29 cells and subjected to dual-luciferase reporter assays.

Assessment of CSN5 activity

Briefly, the assay for hydrolysis of ubiquitin-7-amido-4-methylcoumarin (ubiquitin-AMC) was performed in a 384-well plate in 50 µl reaction buffer (0.1 M Tris-HCl, PH 7.5, 1 mM EDTA, 1 mM dithiothreitol, and 0.1 mg/ml ovalbumin) at 37 °C. After adding of 1 µM CSN5 and 0.2 mM ubiquitin-AMC, the enzyme reaction was started. Assessment of wild-type and △MPN CSN5 activity were based on the level of released AMC from ubiquitin-AMC, measured by fluorescence (λex = 380 nm, λem = 440 nm).

Immunohistochemistry of human colon tumor samples and clinical data

The 254 samples of CRC and 58 adjacent normal formalin-fixed, paraffin-embedded tissues were obtained from patients during operation at Nanjing First Hospital (Nanjing, China). None of these patients received preoperative chemotherapy or radiotherapy. This study was approved by the ethics committee of Nanjing First Hospital and written informed consent was obtained from each patient. Immunohistochemical staining of human colon cancer specimens was performed as previously described [24]. Slices were incubated with CCL5 (Abcam), CD68 (Sigma-Aldrich), p-p65 (Abcam), p-STAT3 (Cell Signaling Technology), CSN5 (Abcam), PD-L1 (Abcam) antibodies, and biotin-conjugated secondary antibody. The avidin-biotin-peroxidase complex was then added for incubation. The CSN5 expression data in Fig. 6g was obtained from TCGA database. Images were taken with a Nikon camera and were analyzed by using Image-Pro Plus 6.0.

In situ hybridization

5-μm-thick tissue sections were deparaffinized in xylene, dehydrated in ethanol of decreasing concentration. Air-dried tissue sections were subjected to heat pre-treatment (microwave oven) and pepsin digestion at 37 °C for 10 min to unmask mRNA targets. After washing with 0.5 M TBS, endogenous peroxidase activity and the unspecific staining were blocked with 3% hydrogen peroxide (10 min) and non-immune sheep serum (30 min), respectively. Serum was removed prior to incubation with anti-CD68 antibody (1:150) overnight. The following day, the sections were incubated with a biotinylated goat anti-mouse/rabbit secondary antibody for 10 min followed by a streptavidin-biotinylated peroxidase complex for another 10 min. After washing with PBS, the sections were processed with diaminobenzidine for 10 s, and then the reaction was stopped by washing with deionized water. Next, the specimens were fixed for 10 min at RT with 1% paraformaldehyde in 0.1 M PBS (PH 7.2–7.6). Prehybridization was done at 37 °C for 4 h by adding 20 μl of prehybridization buffer to each section. For CCL5 mRNA detection, the CCL5 mRNA probe (Boster biological technology) was applied to the tissue sections for co-denaturing the probe and target at 95 °C for 5 min. Then, the hybridization step was performed at 37 °C overnight. The stringent washes were conducted with 2×SSC (5 min, twice), 0.5×SSC (15 min, once), and 0.2× SSC (15 min, once) at 37 °C. Blocking was performed with blocking buffer for 30 min at 37 °C. The blocking buffer was removed prior to implement of the following steps: biotinylated mouse antidigoxigenin antibody for 40 min at 37 °C, SABC-AP for 15 min at 37 °C, enzymatic color development with 5-bromo-4-chloro-30-indolyphosphate and nitro blue tetrazolium (BCIP/NBT) for 2 min at 37 °C. The nuclei were counterstained with Nuclear Fast Red and mounted with Eukitt Mounting Medium. Images were taken with a Nikon camera and were analyzed by using Image-Pro Plus 6.0.

Cellular thermal shift assay (CETSA)

Cellular thermal shift assay (CETSA) was applied to confirm the specificity of C-15 towards CSN5 protein. The CETSA and the isothermal dose response were performed as described [25]. The harvested HT29 cells were dispensed into PCR tubes at a cell density of 50,000 cells per tube in 100 μl of DMEM. The cell suspensions were heated at predetermined temperatures (52, 55, 58, 61, 64, 67, and 70 °C) for 3 min in a 96-well Veriti thermal cycler (Applied Biosystems) followed by 3 min of cooling. Then, the cells were frozen in a CoolSafe Chamber surrounded by dry ice. The cell suspensions were freeze-thawed three times with 15 s of vortexing after each thaw. Cell lysates were centrifuged at 20,000 × *g* for 20 min at 4 °C. The supernatants containing the remaining soluble CSN5 were prepared for western blot analysis.

Statistical analysis

Statistical analyses were performed using GraphPad Prism 6.0. Differences between the different groups were tested using the Student's *t*-test or one-way ANOVA. The correlations were performed using Pearson's chi-square test. Kaplan–Meier method was used to evaluate the survival rate and analyzed by log-rank test. All experimental data were presented as the mean ± S.D. of at least three independent experiments. The differences were considered to be significant at $p < 0.05$. Where statistical significance is evaluated, variance between groups is confirmed to be similar between comparison groups (control vs. experimental) and the statistical analysis is deemed appropriate. For data sets with sufficient *n* to analyze population distribution, tests for normality were administered (Anderson–Darling, D'Agostino & Pearson, Shapiro–Wilk, Kolmogorov–Smirnov).

Results

Macrophage infiltration induced by LPS or HCD promotes CRC by upregulating PD-L1 expression

Given that both HCD and LPS promote macrophage infiltration, we investigated the effect of additional infiltration of macrophages on CRC development. Two macrophage-infiltrating CRC models were constructed (AOM/LPS and

AOM/HCD). As expected, an additional 60-day treatment of LPS or HCD markedly promoted tumor growth (Fig. 1a). We also analyzed the tumor-infiltrating lymphocyte (TIL) population of tumor masses and found that while the number of macrophages ($CD11b^+$ $F4/80^+$) was elevated by LPS or HCD, the cytotoxic T-cell population ($CD8^+$ $IFN\gamma^+$) was remarkably reduced (Fig. 1b, c). Similar results were confirmed in a CT26 allograft model treated with LPS

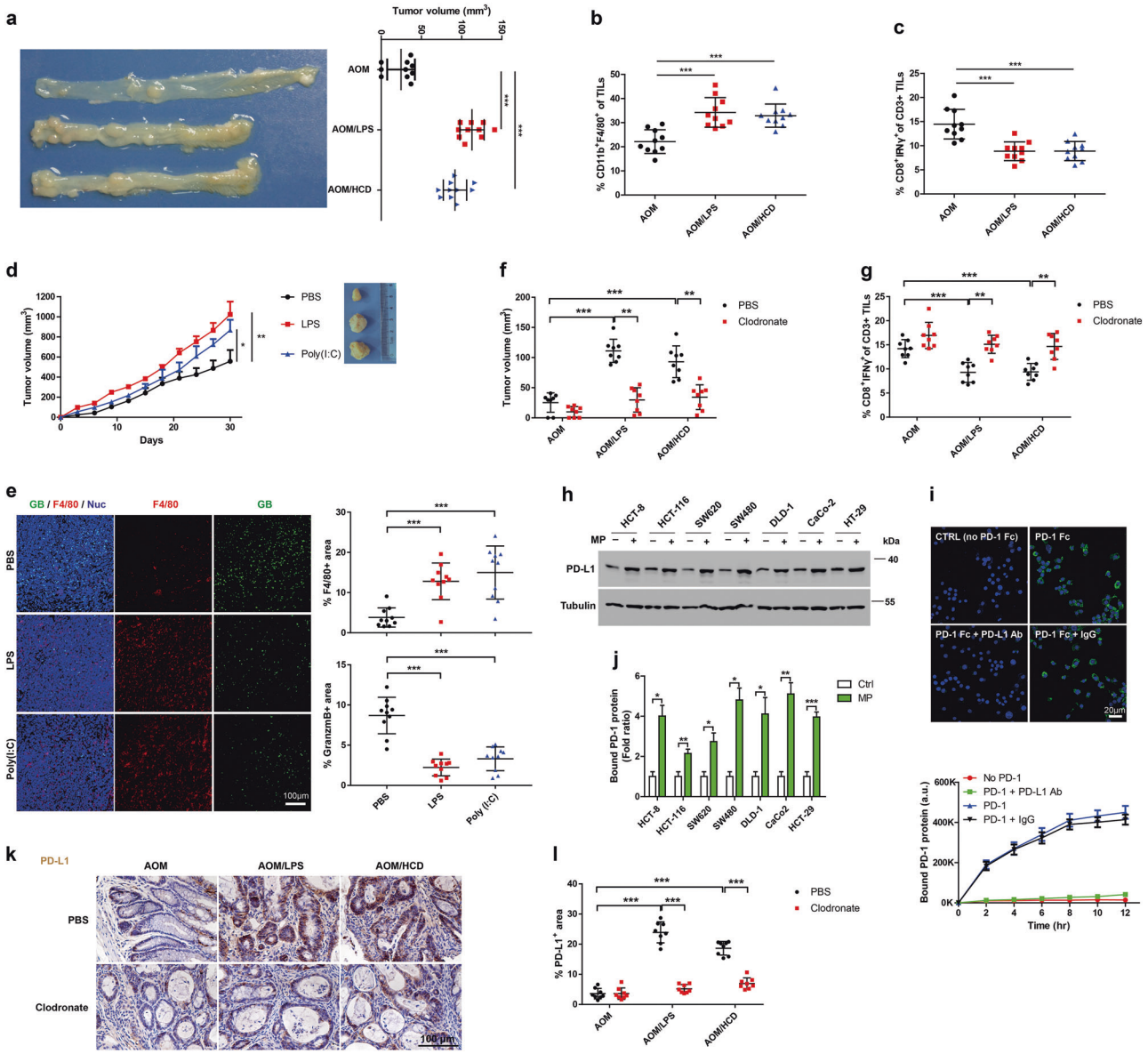

Fig. 1 Macrophage infiltration induced by LPS or HCD promotes CRC by upregulating PD-L1 expression. **a** Tumor volume of C57BL/6 mice treated with AOM alone or in combination with LPS or HCD ($n = 10$ per group). **b** Macrophage ($CD11b^+F4/80^+$) number in $CD45^+$ TILs from colon tumors ($n = 10$). **c** Intracellular cytokine staining of $CD8^+IFN\text{-}\gamma^+$ in $CD3^+$ TILs from colon tumors ($n = 10$). **d** Tumor growth of CT26 cells in C57BL/6 mice following administration with LPS, poly(I:C), or PBS was measured every 3 days ($n = 10$ mice per group). **e** Representative immunofluorescence staining (left) and analysis (right) of F4/80 and granzyme B in CT26 tumors. Scale bar, 100 μm. **f** Tumor volume in AOM, AOM/LPS, and AOM/HCD mice treated with 100 μL of clodronate liposome or PBS liposome ($n = 8$). **g** Intracellular cytokine staining of CD8+IFN-γ+ in $CD3^+$ TILs from colon tumor of AOM, AOM/LPS, and AOM/HCD mice treated with 100 μL of clodronate liposome or PBS liposome ($n = 8$). **h** PD-L1 expression in various colon cancer cells in the presence or absence of MP was measured by western blot. **i** The association of cancer cells (blue signal, dapi) with PD-1 Fc protein (green signal, Alexa 488) during a 12-h period was measured by fluorescence microscope. The images were shown at the top, and quantitative binding of PD-1 Fc protein and PD-L1-expressing cells was shown at the bottom. Scale bar, 20 μm. **j** PD-1 binding capacity of various colon cancer cell lines following addition of MP was examined by PD-L1/PD-1 binding assay. **k** PD-L1 expression measured by IHC in AOM, AOM/LPS and AOM/HCD mice treated with 100 μL of clodronate liposome or PBS liposome ($n = 8$). Scale bars, 100 μm. **l** Quantification of **k** ($n = 8$). Values are mean ± s.d. Results in vitro are representative of three independent experiments and $^*P < 0.05$, $^{**}P < 0.01$, $^{***}P < 0.001$

or poly (I:C) (Fig. 1d, e). These data revealed that macrophages may be related to the development of CRC. To investigate whether macrophage infiltration accounts for the population inhibition of cytotoxic T cells, we depleted macrophages by clodronate liposome (Fig. S1a) and found that both LPS and HCD failed to induce a significant increase of tumor burden and inhibit T cell population (Fig. 1f, g). Therefore, macrophage infiltration in tumor tissue might promote tumor growth by inhibiting cytotoxic T cells.

The binding of PD-L1 on tumor cells to PD-1 on T cells results in exhaustion of T cells, thereby bypassing immune surveillance [26]. We thus asked whether PD-L1 dysregulation in cancer cells is involved in macrophages-mediated tumor growth. Considering that TAMs can suppress the immune response by secreting immunosuppressive factors, LPS-treated inflammatory factor-enriched macrophage-conditioned medium (MP) was collected and applied to various CRC cells. MP markedly increased PD-L1 expression and its PD-1 binding ability in multiple CRC cells (Fig. 1h–j). Furthermore, our in vivo results suggested that LPS and HCD enhanced PD-L1 expression significantly in tumor tissues. However, depletion of macrophages with clodronate liposome attenuated the PD-L1 expression (Fig. 1k, l). These results demonstrated that macrophages may promote CRC development by modulating PD-L1 expression.

Macrophages-secreted CCL5 exert an immunosuppressive effect via PD-L1 regulation

To identify the factor responsible for PD-L1 upregulation, macrophages were treated with PBS, LPS, or poly (I:C) for 12 h. The supernatant was collected and subjected to ELISA assay. We found that poly (I:C) and LPS enhanced the expression of CCL5, TNF-α, IL-1β, C-X-C motif chemokine ligand 3 (CXCL3), IL-6, and IL-8 (Fig. 2a). However, only the anti-CCL5 antibody inhibited both the MP-induced elevated PD-L1 protein level and its PD-1 binding (Fig. 2b, c). To confirm the role of CCL5 in PD-L1-mediated suppression of cytotoxic T-cell activity, HT29 cells were co-cultured with activated T cells. T cell-mediated killing of HT29 cells was markedly suppressed by MP, however, anti-CCL5 antibody abrogated the effect of MP (Fig. 2d, e). When PD-L1 was knocked down in HT29 cells, neither MP exposure nor CCL5 antibody treatment affected the killing ability of T cells (Fig. 2e), suggesting that T cell-mediated killing of tumor cells is dependent on PD-L1. Collectively, these data indicated that CCL5 is the major inflammatory factor that upregulates PD-L1 expression and inhibits cytotoxic T-cell activity in vitro.

To clarify the source of CCL5, we depleted macrophages in the AOM/LPS (HCD) model of CRC (Fig. S1a). A significant reduction in serum and colonic CCL5 levels was observed (Fig. S1b and Fig. 2f). The mRNA in situ hybridization results revealed that the CCL5 transcript level was high in stromal cells, and particularly in CD68-positive cells (Fig. 2g, h). We next validated the role of CCL5 in vivo. The anti-CCL5 antibody attenuated the tumor burden and restored the activity of cytotoxic T cells (Fig. 2i–l). Intriguingly, anti-CCL5 also reduced the AOM/LPS-induced infiltration of macrophages (Fig. 2m). CCL5 recruits regulatory T (Treg) cells into tumor masses [27], which prompted us to investigate the frequency of $FoxP3^+$ Treg cells. The anti-CCL5 antibody did not alter the number of Treg cells ($CD25^+FoxP3^+$) (Fig. 2n). We then validate the CCL5-mediated upregulation of PD-L1 in vivo by exogenous administration of CCL5 and anti-PD-1. CCL5 ameliorated clodronate-induced inhibition of tumor burden and colonic CCL5 level and decreased the frequency of $CD8^+$ T cells, while anti-PD-1 had opposite effect in aspect of tumor growth and $CD8^+$ T cells (Fig. S1c–e). Strikingly, neither CCL5 nor anti-PD-1 treatment rescued the macrophage density (Fig. S1f), indicating potent depletion of macrophages by clodronate liposomes. Taken together, these results indicated that macrophages exert an immunosuppressive effect by secreting CCL5, and that this effect is dependent on PD-L1 expression.

Nuclear translocation of p65 and STAT3 is involved in CCL5-induced PD-L1 upregulation

CCL5 increases the activity of many signaling pathways, such as the PI3K/AKT, ERK, STAT3, and NF-κB pathways [28–30]. Therefore, we applied inhibitors to identify the signaling pathway implicated in CCL5-induced PD-L1 upregulation. Importantly, three inhibitors—IKKβ inhibitor Bay 11-7082, STAT3 inhibitor niclosamide, and NF-κB inhibitor parthenolide—significantly reduced the PD-L1 level (Fig. 3a). Upon CCL5 stimulation, p65 and STAT3 translocated to the nucleus at 1 h; translocation peaked at 6 h. And as the expression of nuclear p65 and STAT3 increased, the protein level of PD-L1 on the membrane also increased (Fig. 3b), indicating that nuclear p65 and STAT3 are involved in the upregulation of PD-L1. We used shRNA targeting p65 and STAT3 to further confirm this result (Fig. 3c). To determine how CCL5 upregulates PD-L1 expression, we evaluated the PD-L1 mRNA level in HT29 cells. Unlike IFN-γ, which enhances PD-L1 expression at the transcriptional level [31], CCL5 had little effect on the mRNA level of PD-L1 (Fig. 3d), implying that CCL5 might increase the PD-L1 protein level by a posttranslational mechanism.

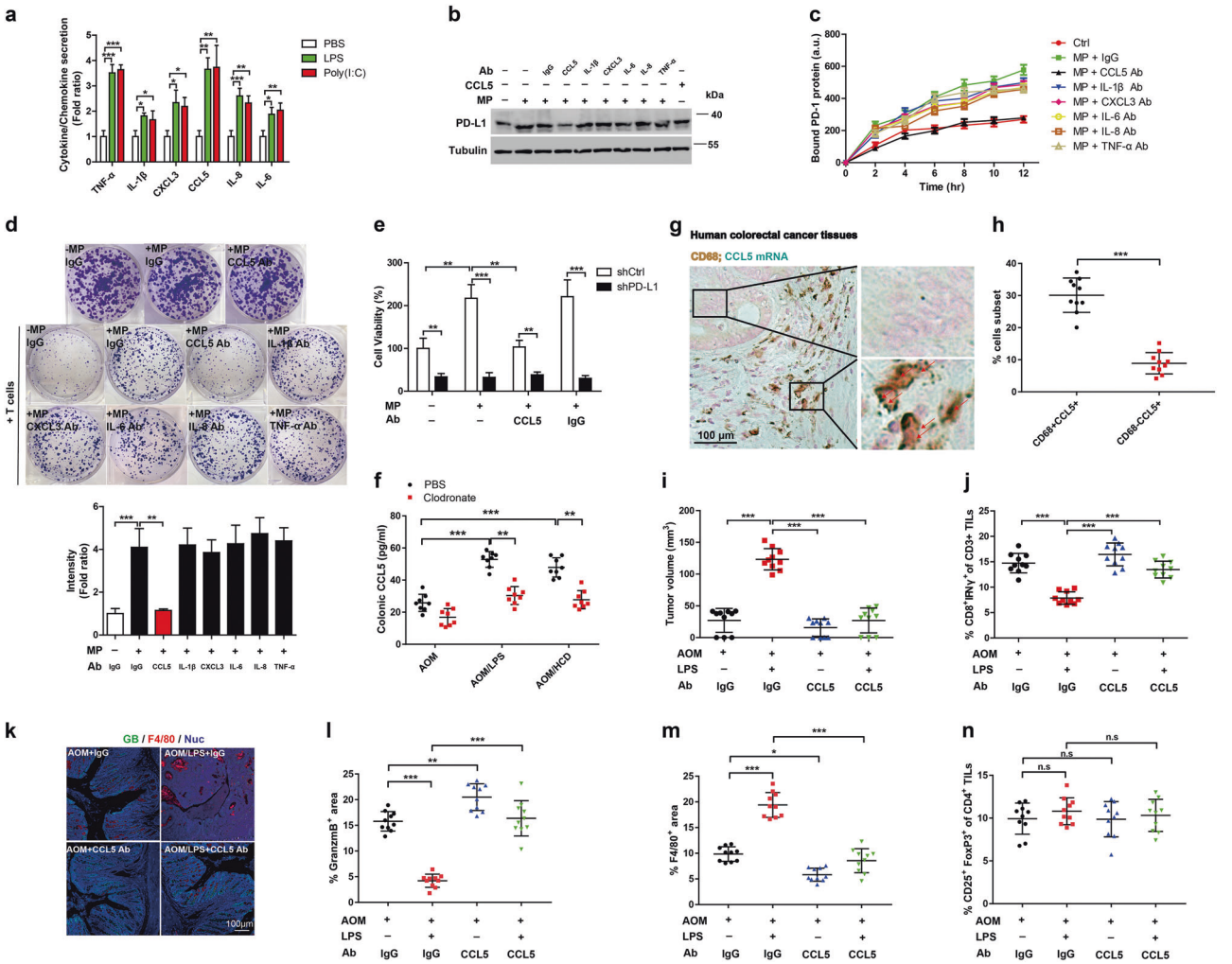

Fig. 2 Macrophages-secreted CCL5 exert an immunosuppressive effect via PD-L1 regulation. **a** Quantification of CCL5, IL-1β, CXCL3, IL-6, IL-8, TNF-α with ELISA assay secreted from PBS-, LPS-, or poly(I:C)-treated macrophages. **b** PD-L1 protein expression in HT29 cells treated with neutralizing antibodies of the indicated chemokines/cytokines. **c** PD-1 binding affinity of HT29 cells co-treated with MP and antibodies of the indicated chemokines/cytokines. **d** T cell-regulated tumor cell killing assay in HT29 cells treated with MP and neutralization antibodies for the indicated chemokines/cytokines. Activated T cell and HT29 cells were co-cultured in six-well plates for 7 days and then surviving HT29 cells were visualized by crystal violet staining. Relative fold ratios of surviving cell intensities are shown. **e** T cell-mediated HT29 cells killing analysis measured by CCK8 assay. PD-L1 of HT29 cells were deleted using shRNA assay. **f** Colonic CCL5 levels measured by ELISA assay in AOM, AOM/LPS, and AOM/HCD mice treated with 100 μL of clodronate liposome or PBS liposome ($n = 8$). **g** Representative immunohistochemistry staining for CD68 combined with CCL5 RNA in situ hybridization in human colorectal cancer tissue. Scale bar, 100 μm. Arrows indicate CCL5 mRNA ISH ($n = 10$). **h** Quantification of (**g**) ISH shows large clusters of hybridized CCL5 probe in CD68-positive cells, indicating CCL5 mRNA is mainly expressed in CD68-positive cells ($n = 10$). **i** Tumor volume of AOM/LPS model following treatment with IgG or CCL5 antibody ($n = 10$). **j** Intracellular cytokine staining of CD8+IFN-γ+ in $CD3^+$ TILs of AOM/LPS tumors ($n = 10$) treated with IgG or CCL5 antibody. **k** Immunofluorescence staining of F4/80 and granzyme B in AOM/LPS tumors. Scale bar, 100 μm. **l**, **m** Statistical analysis of granzyme B and F4/80 in **k** ($n = 10$). **n** FACS quantification of the percentage of $CD25^+FoxP3^+$ cells in $CD4^+$ TILs of AOM/LPS tumors ($n = 10$) treated with IgG or CCL5 antibody. Values are mean ± s.d. Results in vitro are representative of three independent experiments and $^*P < 0.05$, $^{**}P < 0.01$, $^{***}P < 0.001$

CSN5 deubiquitinates and stabilizes PD-L1 in CCL5-stimulated CRC cells

During ubiquitination, the most studied posttranslational modification, Ub is conjugated to a target protein to regulate its degradation. In the DUB family, Ub-specific proteases and JAMM-motif proteases are associated with protein stabilization [32, 33]. Therefore, we analyzed the mRNA levels of common DUBs to identify those involved in the posttranslational regulation of PD-L1. High expression of CSN5 was observed in vitro and in vivo, and this effect was reversed by a STAT3 or NF-κB/p65 inhibitor (Fig. 4a and Fig. S2c). These data indicated that CSN5 participates in CCL5-mediated upregulation of PD-L1 by interacting with STAT3 and p65. Also, we used shCSN5 to confirm this result (Fig. 4b).

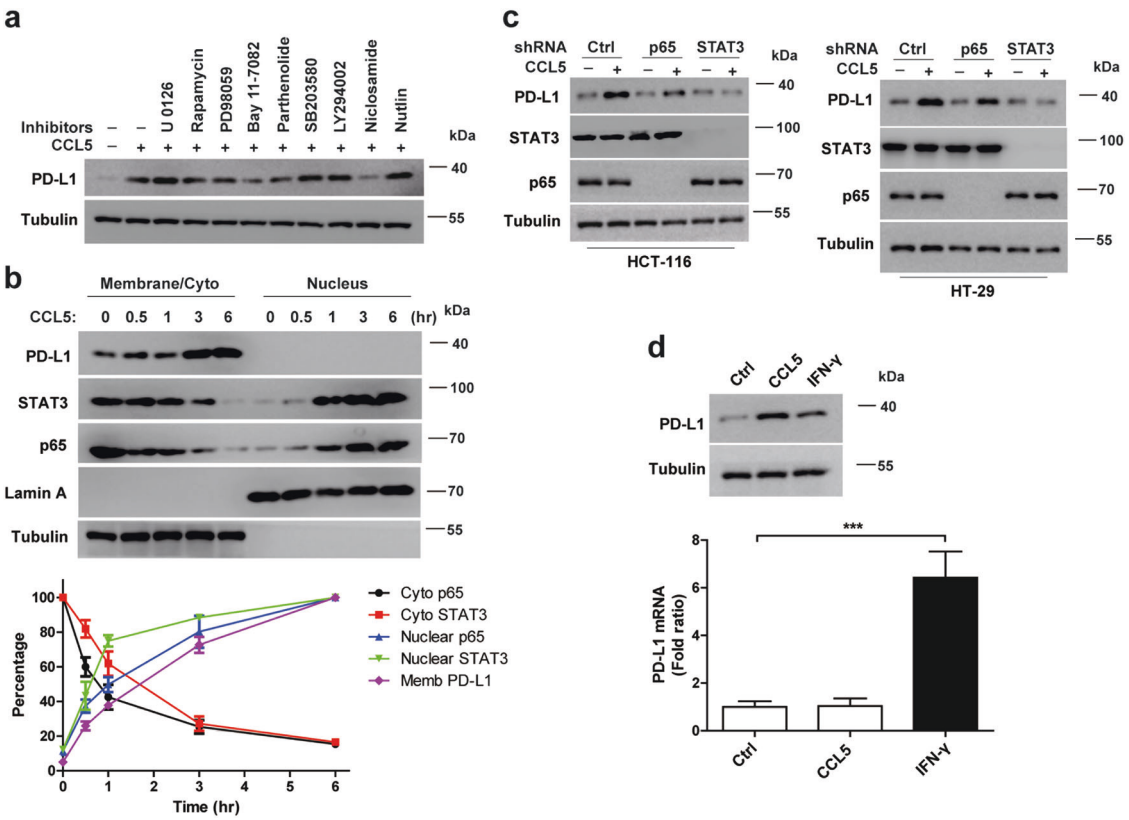

Fig. 3 Nuclear translocation of p65 and STAT3 is involved in CCL5-induced PD-L1 upregulation. **a** PD-L1 expression detected by western blot in HT29 cells pretreated with the indicated inhibitors for 45 min, followed by CCL5 (25 ng/ml) treatment for 8 h. **b** Nuclear translocation of p65 and STAT3 at pre-decided time points in CCL5 -treated HT29 cells. Protein expression is shown on the top, dynamic protein expression was shown at the bottom. **c** PD-L1 expression in p65- or STAT3-deleting HCT116 and HT29 cells after TNF-α treatment for 8 h. **d** Western blot analysis of PD-L1 in HT29 cells treated with CCL5 or IFN-γ was shown on the top, and qRT-PCR of PD-L1 mRNA was shown at the bottom. Values are mean ± s.d. Results are representative of three independent experiments and $*P < 0.05$, $**P < 0.01$, $***P < 0.001$

This result was supported by double immunofluorescence staining, which showed co-localization of CSN5 and PD-L1 in HCT116 cells (Fig. 4c). Furthermore, by half-life assay, we found that PD-L1 was rapidly degraded in CSN5-deficient cells (Fig. 4d). Next, we assessed the deubiquitination of PD-L1 by CSN5 using the proteasome inhibitor MG-132. While MG-132 significantly enhanced the accumulation of Ub-PD-L1, it was markedly reduced by CSN5 overexpression or CCL5 treatment (Fig. 4e).

Because the deubiquitinating activity of the CSN family is dependent on the JAMM/MPN+ motif of the metalloprotease complex [34], we asked whether the MPN domain of CSN5 is responsible for the deubiquitination of PD-L1. Wild-type CSN5, rather than MPN motif-deleted CSN5 (designated △MPN), stabilized PD-L1 protein (Fig. 4f). Consistently, the results of a cell-free deubiquitination assay revealed that CSN5 significantly reduced the basal ubiquitination of PD-L1 (Fig. 4g). Next, we confirmed that the MPN domain was critical for CSN5 activity by measuring AMC release from Ub-AMC (see "Materials and methods" section) (Fig. 4h). Also, wild-type CSN5, but not △MPN, induced a dose-dependent reduction in the level of Ub-PD-L1 (Fig. 4i). Therefore, CSN5, via its MPN motif, plays a role in CCL5-mediated PD-L1 stabilization by deubiquitinating PD-L1.

Formation of the p65/STAT3 complex activates CSN5 transcription

The results above prompted us to investigate the association between p65, STAT3, and CSN5 in CCL5-mediated stabilization of PD-L1. We hypothesized that p65 and STAT3 together regulate CSN5 expression at the transcriptional level. Similar to CHX, a protein synthesis inhibitor, the transcription inhibitor actinomycin D also inhibited the expression of PD-L1 in colon cancer cells pretreated with CCL5 (Fig. 5a). This suggests that the transcriptional activation of CSN5 is required for PD-L1 stabilization. Moreover, the CSN5-promoter-luciferase (CSN5-Luc) showed robust responses to CCL5, however, niclosamide or/and Bay 11-7082 impaired this responsivity (Fig. 5b). We knocked out endogenous STAT3 and p65 in HEK293 cells

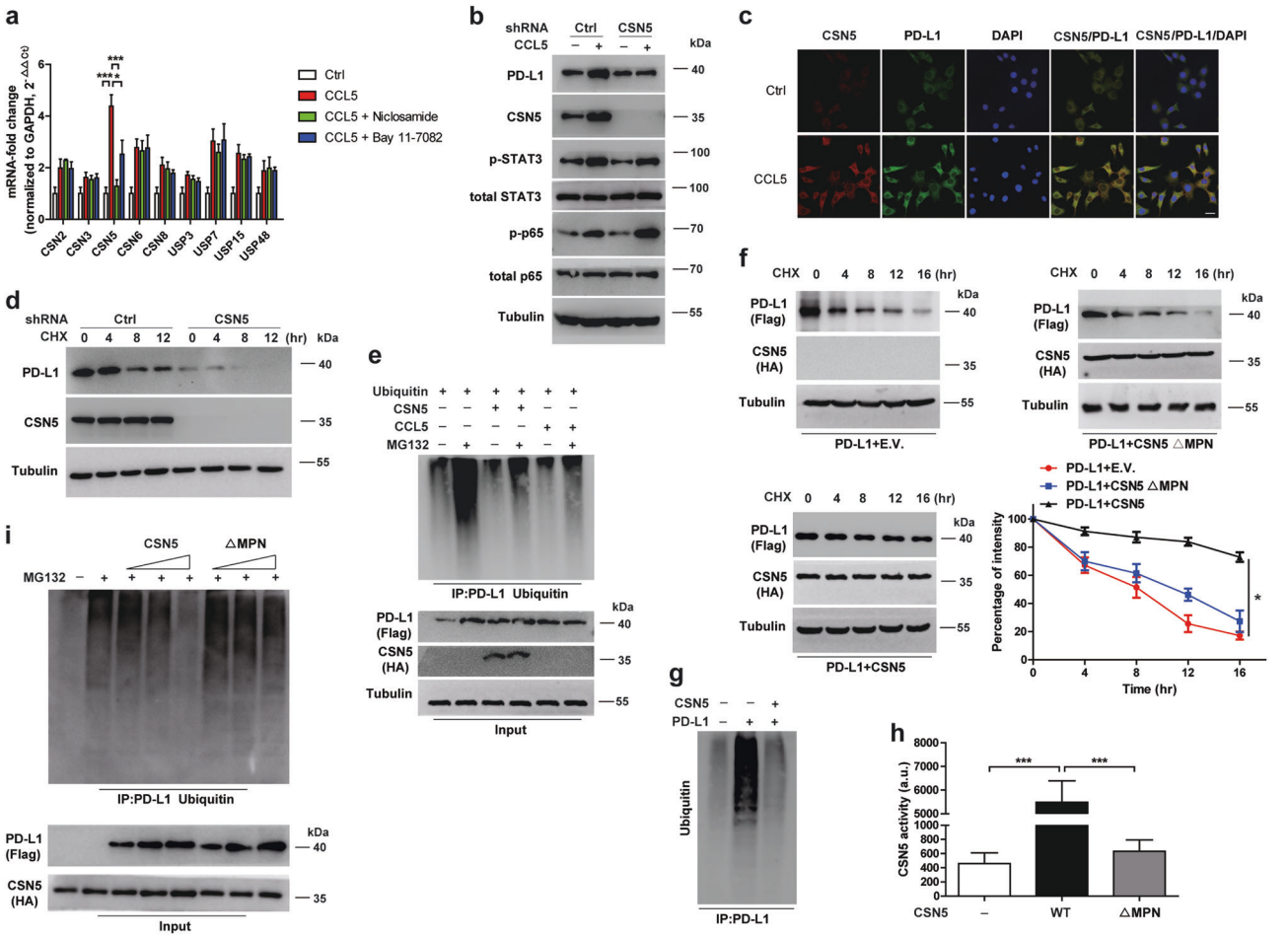

Fig. 4 CSN5 deubiquitinates and stabilizes PD-L1 in CCL5-stimulated CRC cells. **a** qRT-PCR analysis of the deubiquitinating enzymes in HT29 cells, which were pretreated with 1 μM niclosamide overnight or 10 μM Bay 11-7082 for 1 h, followed by treatment with CCL5 (25 ng/ml) for 8 h. Results are normalized to GAPDH. **b** Western blot analysis of PD-L1, p65, and STAT3 expressions in CSN5-deleted HT29 cells after CCL5 stimulation. **c** Immunofluorescence staining of CSN5 (red) and PD-L1 (green) in HCT116 cells. Scale bar, 20 μm. **d** Protein stability of PD-L1 in CSN5-deleted HT29 cells. Cells were co-incubated with cycloheximide (CHX, 50 μg/ml) at the indicated time points prior to western blot analysis. **e** Ubiquitination assay of PD-L1 in HEK293 cells in response to treatment with 10 μM MG-132 for 3 h or CCL5 (25 ng/ml) for 8 h. Cells were transfected with ubiquitin or CSN5 constructs. Ubiquitinated PD-L1 was immunoprecipitated (IP) prior to western blot analysis with the ubiquitin antibody. **f** Protein stability of PD-L1 in HEK293 cells transfected with Flag-PD-L1 and WT HA-CSN5 or MPN-deleted (△MPN) CSN5. E.V., empty vector. **g** Cell-free deubiquitination assay of PD-L1. Purified CSN5, PD-L1, ubiquitin, E1, E2, and ATP were incubated at 37 °C for 2 h and then analyzed with western blot. **h** Activity of wild-type CSN5 and △MPN CSN5 were measured by the level of released AMC from ubiquitin-AMC, a fluorogenic substrate. **i** Ubiquitination assay of PD-L1 in HEK293 cells transfected with WT CSN5 or MPN-deleted (△MPN) CSN5 plasmids. Values are mean ± s.d. Results are representative of three independent experiments and $^{*}P < 0.05$, $^{**}P < 0.01$, $^{***}P < 0.001$

and subsequently reconstituted them with overexpression plasmids. Interestingly, the overexpression of p65 alone failed to activate CSN5 transcription, whereas co-reconstitution of p65 and STAT3 markedly increased CSN5-Luc activity in CCL5-treated cancer cells (Fig. 5c). These data demonstrated that p65 acts as a co-activator of STAT3 to promote CSN5 transcription.

To identify the STAT3-binding site in the CSN5 promoter region, a luciferase reporter assay was performed. Deletion of the region −219 to −91 resulted in the loss of luciferase activity in HT29 cells stimulated with CCL5 (Fig. 5d). In addition, STAT3 bound to the 'ttcaacaaa' site of the CSN5 promoter, while p65 bound to it only in the presence of STAT3 (Fig. 5e). Consistently, an interaction between p65 and STAT3, which was significantly enhanced by CCL5, was detected in the nuclear extract of HT29 cells by coimmunoprecipitation assay (Fig. 5f). These results demonstrated that p65 binds to STAT3 to activate CSN5 expression at the transcriptional level in CRC cells.

To confirm the role of the STAT3/p65 complex in CSN5-mediated stabilization of PD-L1, overexpression plasmids of p65 and STAT3 were employed. We observed an increase in PD-L1 level and its binding ability to PD-1.

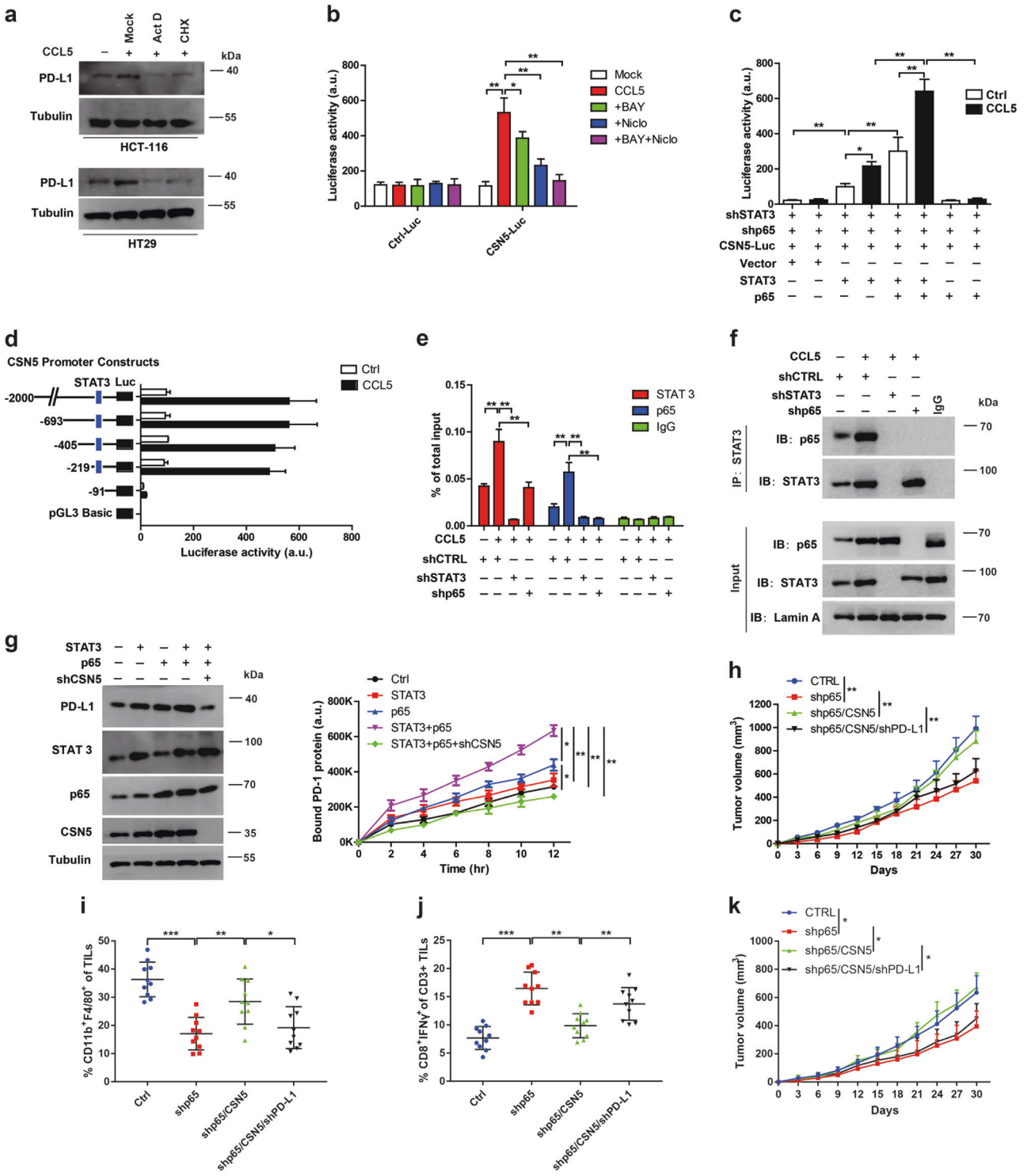

However, these effects were abolished by the knockdown of CSN5 (Fig. 5g). Furthermore, the knockout of p65 in allograft models reduced tumor growth and macrophage infiltration and increased $CD8^+$ T cell activity, but these effects were reversed by the overexpression of CSN5. Moreover, further downregulation of PD-L1 attenuated CSN5-mediated tumorigenesis (Fig. 5h–j). Consistent with the above, expression of F4/80, CCL5, p-p65, p-STAT3, CSN5, and PD-L1 was significantly higher in AOM/LPS and AOM/HCD colon tumor tissue than in AOM colon tumor tissue (Fig. S2a, b). Interestingly, this p65/STAT3-CSN5-PD-L1 pathway was functional even without LPS challenge (Fig. 5k). These data indicated that formation of the p65 and STAT3 complex upregulates CSN5 expression,

◀ **Fig. 5** Formation of the p65/STAT3 complex activates CSN5 transcription. **a** Western blot analysis of PD-L1 expression in HCT116 and HT29 treated with 0.5 μg/ml Act D or CHX (50 μg/ml) for 4 h. **b** Luciferase activity from the indicated groups in HT29 cells transfected with CSN5 luciferase promoter (CSN5-Luc), which was normalized to Renilla luciferase. **c** Luciferase activity analysis in HEK293 cells. Endogenous STAT3 and p65 in HEK293 cells were first deleted by shRNA, and subsequently reconstituted with the indicated overexpressed plasmid. **d** Progressive deletions of the 5′-region of the CSN5 promoter in luciferase (Luc) constructs were transfected into HT29 cells and subjected to luciferase reporter assays. **e** The binding of STAT3 and p65 to the CSN5 promoter was analyzed using chromatin immunoprecipitation assay. Mouse immunoglobulin G (IgG) was used as a negative control. **f** Nuclear lysates were analyzed for the interaction of p65 and STAT3 by immunoprecipitation in HT29 cells treated with the indicated factors. **g** Western blot analysis of PD-L1 expression in HT29 cells transfected with the indicated plasmids (left). Results of the PD-1/PD-L1 binding assay (right). **h** Tumor growth of CT26 cells in LPS-treated C57BL/6 mice. Tumor growth was measured every 3 days ($n = 10$ mice per group). **i**, **j** FACS quantification of the frequency of macrophages and $CD8^+$T cells in LPS-treated C57BL/6 mice. **k** Tumor growth of CT26 cells in C57BL/6 mice without LPS stimuli. Tumor growth was measured every 3 days ($n = 10$ mice per group). Values are mean ± s.d. Results in vitro are representative of three independent experiments and $^*P < 0.05$, $^{**}P < 0.01$, $^{***}P < 0.001$

which is critical for CCL5-mediated stabilization of PD-L1 and tumor growth.

Expression of PD-L1 associates with p-p65, p-STAT3, CSN5, and high CSN5 expression is predictive of a poor prognosis in patients with CRC

We next investigated the levels of the involved protein in CRC cell lines and human CRC specimens. Western blotting indicated that the PD-L1 protein level in these cell lines was positively correlated with CSN5, p-p65, and p-STAT3 levels (Fig. 6a). The immunohistochemical staining results revealed that CCL5, CD68 (macrophage marker), p-p65, p-STAT3, and CSN5 expression was significantly higher in tumor tissues than in adjacent tissues. By contrast, the number of cytotoxic T lymphocytes ($CD8^+$ granzyme B^+) was significantly lower in colon tumor tissue compared with adjacent normal tissue (Fig. 6b, c). Because stromal PD-L1 plays an important role in CRC, we analyzed the localization of PD-L1 by immunohistochemical (Fig. 6b, c) and

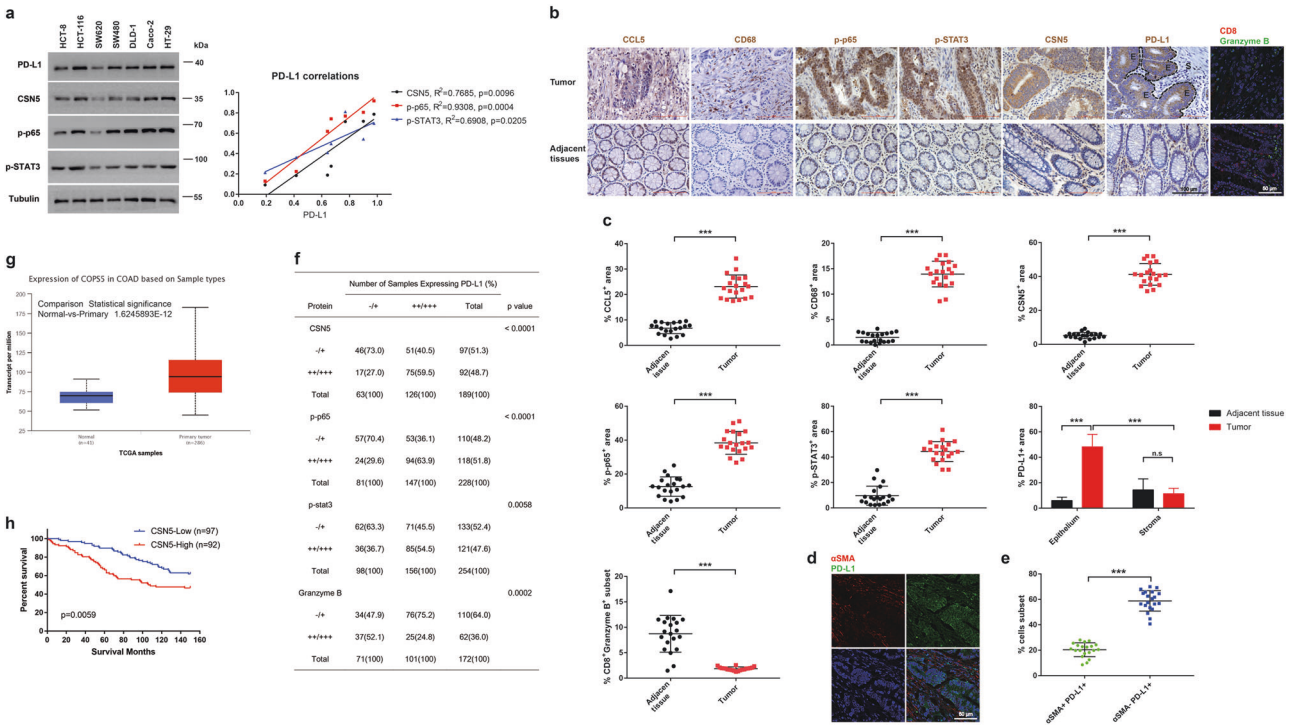

Fig. 6 Expression of PD-L1 associates with p-p65, p-STAT3, CSN5, and high CSN5 expression is predictive of a poor prognosis in patients with CRC. **a** Western blot analysis of the expressions of PD-L1, CSN5, p-p65, and p-STAT3 in seven colon cancer cell lines (left). Simple linear regression between PD-L1 expression and CSN5, p-p65, and p-STAT3 in seven colon cancer cell lines (right). **b** Representative immunohistochemical staining (Scale bars, 100 μm) or immunofluorescence staining (Scale bars, 50 μm) of CCL5, CD68, p-p65, p-STAT3, CSN5, PD-L1, and granzyme B in human colon cancer specimens. The area marked "S" represents stroma, and the area marked "E" represents tumor epithelium. **c** Statistical analysis of **b**. **d** Representative immunofluorescence staining of αSMA (red) and PD-L1 (green) in human colorectal cancer specimen. **e** The percentage of $\alpha SMA^+PD\text{-}L1^+$ and $\alpha SMA^-PD\text{-}L1^+$ cell subset in **d**. Scale bar, 20 μm. **f** Correlations between expression levels of CSN5, PD-L1, p-p65, p-STAT3 and granzyme B expression in surgical specimens of colorectal cancer analyzed using the Pearson chi-square test. **g** CSN5 gene expression in normal colon tissue and primary tumors using the UALCAN gene expression tool (http://ualcan.path.uab.edu). **h** Overall survival of patients with colorectal cancer whose specimens were used in our analysis ($n = 189$). Values are mean ± s.d. Results in vitro are representative of three independent experiments and $^*P < 0.05$, $^{**}P < 0.01$, $^{***}P < 0.001$

double immunofluorescence staining (Fig. 6d, e). PD-L1 was localized to the tumor epithelium rather than the stroma (αSMA^+). IHC results showed that CSN5 was present in 75 (59.5%) of the 126 samples with high PD-L1 expression but in only 51 (40.5%) with low expression of PD-L1, suggesting a positive correlation between the expression of CSN5 and PD-L1 ($p < 0.0001$). Moreover, PD-L1 expression was positively correlated with p-p65 and p-STAT3 expression ($p < 0.0001$ and $p = 0.0058$) but inversely correlated with granzyme B expression ($p = 0.0002$; Fig. 6f). To validate the role of CSN5 in human CRC, we analyzed CRC transcriptome data using the UALCAN gene expression tool (http://ualcan.path.uab.edu). As expected, expression of CSN5 was higher in tumors than in normal specimens (Fig. 6g). Importantly, Kaplan–Meier survival analysis showed that CRC patients with high CSN5 expression had worse overall survival than those with low CSN5 expression (Fig. 6h). These results supported the notion that the p65/STAT3-CSN5-PD-L1 pathway is involved in the progression of human CRC.

CSN5 inhibitor suppresses the growth of CRC

As PD-L1 stability is modulated by CSN5 (Fig. 4), we determined whether PD-L1 destabilization induced by a CSN5 inhibitor would enhance antitumor immunity. Because the MPN domain of CSN5 plays a key role in PD-L1 deubiquitination, we focused on the MPN motif to identify inhibitors of CSN5. Compound-15 (C-15) had a binding energy of −13.4 kcal/mol to CSN5. During binding to the active site of the enzyme, the indazole moiety was bound in the catalytic center of CSN5 through a dual interaction. N2 coordinated to the active site Zn^{2+} in a moderate manner, while the NH formed a tight hydrogen bond with the O of the Asp151 carboxylate. The distal phenyl ring was orientated towards a lipophilic cavity (PDB code, 5M5Q) (Fig. 7a). Furthermore, the interaction between CSN5 and C-15 was detected by CETSA, a recently developed method that allows rapid and simple assessment of target binding of compounds in cells. The results implied that C-15 specifically targets CSN5 in HT29 cells (Fig. S3c, d).

Based on its potential for cancer therapy, we evaluated the effect of C-15 in vivo and in vitro. Importantly, C-15 markedly inhibited Cul1 deneddylation, CSN5 expression, and PD-L1 protein synthesis in seven CRC cell lines and restored the CCL5-mediated reduction of the cytotoxic effect of T cells (Fig. 7b and Fig. S3a, b). However, a shCSN5 and PD-L1-overexpression plasmid abrogated the elevated T cell-mediated killing of HT29 cells induced by C-15 (Fig. S3a, b), revealing a crucial role for the CSN5-PD-L1 axis in C-15-induced activation of T cells. Similar to the in vitro results, the tumor burden and PD-L1 and CSN5 protein levels were significantly reduced in AOM/LPS mice upon treatment with C-15. These mice also showed increased activation of $CD8^+$ T cells (Fig. 7c–e). In an allograft model, C-15 markedly inhibited tumor growth and elevated the activity of cytotoxic T cells. However, overexpression of PD-L1 and the knockdown of CSN5 abrogated the antitumor effect of C-15 (Fig. 7f–h and Fig. S3e). Furthermore, C-15 failed to inhibit tumor growth in $Rag1^{-/-}$ mice and $CD8^+$ T cell-depleted mice (Fig. 7i and S3f), indicating that the tumor-suppressive effect of C-15 is dependent on $CD8^+$ T cells. Together, these results demonstrated that C-15 shows great promise for the treatment of CRC.

Discussion

Our findings revealed a novel mechanism of immune escape involving macrophages, CRC cells, and $CD8^+$ T cells, in which infiltration of macrophages inhibits the $CD8^+$ T-cell response via the CCL5-mediated p65/STAT3-CSN5-PD-L1 pathway in tumor cells and thus promotes the progression of CRC (Fig. 7j). Unexpectedly, the infiltration of macrophages was decreased upon anti-CCL5 and C-15 treatment (Figs. 2m and 7g). One possible explanation is that PD-L1 expression in cancer cells promotes the recruitment of macrophages, because it was correlated with macrophage infiltration in hepatocellular carcinoma (HCC) tissue [8] and blocking of PD-L1 in HCC cells by anti-PD-L1 moderately decreased infiltration of TAMs and increased that of CD8 cytotoxic T lymphocytes [35]. This hypothesis, which warrants further exploration, was supported by our results. First, the knockdown of PD-L1 reduced macrophage infiltration (Fig. 5i). Second, C-15 did not decrease the macrophage density (Fig. 7g) in mice administered PD-L1-overexpressing cancer cells (Fig. 7h). We propose that CCL5 secreted by macrophages induces the upregulation of PD-L1 in cancer cells, which in turn promotes the infiltration of macrophages, forming a positive feedback loop that facilitates immune escape of cancer cells and subsequently the growth of CRC.

A number of studies have focused on the complex crosstalk between TAMs and $CD8^+$ T cells [5]. For example, Peranzoni et al. demonstrated that macrophage depletion increased the average speed and displacement length of $CD8^+$ T cells in MMTV-PyMT mice, resulting in a marked increase in the percentage of $CD8^+$ T cells at the tumor site [36]. This work provides evidence that macrophages are an important determinant of a T cell-excluded tumor phenotype. Furthermore, Lim et al. showed that TNF-α from macrophages elevated PD-L1 expression in breast cancer cells by activating NF-κB [14]. While much work has focused on macrophage-mediated escape of

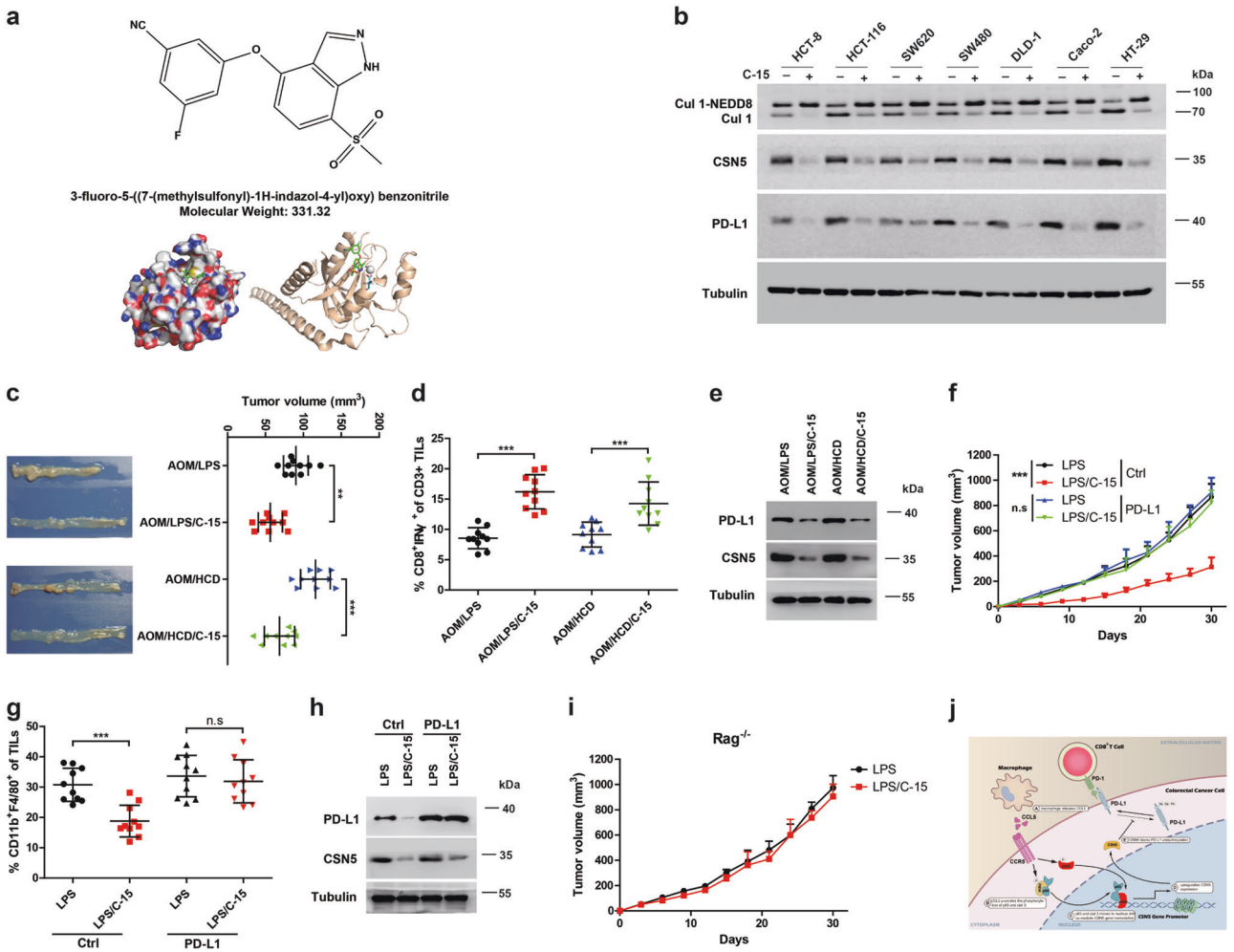

Fig. 7 CSN5 inhibitor suppresses the growth of CRC. **a** Chemical formula of C-15 and the binding mode of C-15 and CSN5 protein. N2 coordinated to the active site Zn2+ in a moderate manner, while the NH forms a tight hydrogen bond with O of the Asp151 carboxylate. **b** Immunoblotting for Cul1, CSN5, and PD-L1 in seven CRC cell lines after treatment with C-15 (1 μM) for 24 h. **c** Tumor volume of AOM/LPS and AOM/HCD mice following oral administration with C-15 (20 mg/kg, 88 days) were measured ($n = 10$ mice per group). **d** Intracellular cytokine staining of CD8+IFN-γ+ in $CD3^+$ TILs in tumors ($n = 10$). **e** Western blot analysis for PD-L1 and CSN5 expressions in tumors from the indicated groups ($n = 5$). **f** Tumor growth of CT26 cells (transfected with ctrl or PD-L1 overexpression plasmid) in C57BL/6 mice following oral administration with C-15 (20 mg/kg, 30 days) was measured every 3 days ($n = 10$ mice per group). **g** Intracellular cytokine staining of CD8+IFN-γ+ in $CD3^+$ TILs from allografts ($n = 10$). **h** Western blot analysis of PD-L1 and CSN5 expressions in allografts from the indicated groups ($n = 5$). Values are mean ± s.d. Results in vitro are representative of three independent experiments and $^*P < 0.05$, $^{**}P < 0.01$, $^{***}P < 0.001$. **i** Tumor growth of CT26 cells in Rag1 knockout mice treated with PBS or C-15. ($n = 10$). **j** Graphical abstract

cancer cells from immune surveillance, how macrophage-secreted cytokines suppress $CD8^+$ T cells in CRC is unclear. Using neutralizing antibodies, we found that CCL5, but not other chemokines secreted from macrophages, plays an immunosuppressive role in the CRC microenvironment. The CCL5-CCR5 axis has been reported to direct Treg cell homing to tumors, and inhibition of this signaling axis shows promise as a novel strategy for cancer treatment [27]. To investigate whether CCL5-dependent homing of Treg cells is involved in the observed immunosuppression, we evaluated the number of Treg cells in AOM/LPS tumors. Neither LPS nor an anti-CCL5 antibody altered the percentage of $Foxp3^+$ Treg cells. This finding confirmed the role of suppression of $CD8^+$ T cells in CCL5-mediated immune escape.

Consistent with our results, Zhang et al. demonstrated that CCL5 deficiency enhances $CD8^+$ T cells infiltration in $CCL5^{-/-}$ mice, suggesting a correlation between inhibition of T-cell immunity and CCL5 [7]. However, we found that the expression level of PD-L1/PD-1 in TILs of $CCL5^{-/-}$ mice was increased, which is inconsistent with the upregulation of PD-L1 in tumor cells. There are several explanations for the discrepancy. First, as Lee et al. concluded [37], PD-L1 expression in tumor cells and TILs may involve different mechanisms. Second, we used CRC models treated with LPS or other stimuli, while the animal

model in Zhang's paper lacked these stimuli. Overall, our study in combination with Zhang's work showed that CCL5 promotes tumor progression by modulating immunosuppression in the TME.

In the current study, CCL5 derived from TAMs promoted not only the expression of PD-L1 but also PD-1/PD-L1 interaction. PD-L1/PD-1 immune checkpoint inhibitors are effective against melanoma, renal carcinoma, and non-small-cell lung cancer. However, this therapeutic strategy is effective against only the microsatellite-instability (MSI) subset of CRC, characterized by deficiency of mismatch repair protein [38]. Conversely, microsatellite-stable (MSS) CRC, which has functional mismatch repair mechanism, shows a less marked response to anti-PD-1 therapy. This may result from the immunosuppressive TME, which counteracts antitumor immunity, and poorly antigenic cancer cells [39]. We observed that CCL5 induced a significant increase in PD-L1 expression in CRC cells, irrespective of the microsatellite status in HT29 (MSS) and HCT116 (MSI) cells. Therefore, the novel pathway of PD-L1 upregulation may enhance the treatment of CRC, particularly MSS CRC.

CCL5 activates the NF-κB signaling pathway, which is constitutively activated in tumors [40]. However, in this study, NF-κB/p65 alone did not significantly activate CSN5 transcription, while co-reconstitution of p65 and STAT3 markedly increased the CSN5-Luc activity. The interaction of STAT3 with NF-κB is suggested to be associated with several tumors, such as melanoma and prostate cancer. Furthermore, STAT3 signaling maintains tumor NF-κB activity by promoting RelA acetylation [41]. Our data showed that p65 coactivates STAT3, leading to synergistic promotion of CRC development in an inflammatory context by inducing CSN5 transcription.

We also demonstrated that CCL5 stabilizes PD-L1 by inducing CSN5 expression. Indeed, CSN5 and CSN6, which have an MPN domain, are potential oncogenes and are upregulated in several types of cancer [42–44]. In consequence, inhibition of these two subunits of the COP9 signalosome may have therapeutic potential for human cancer. Several inhibitors of CSN5 reportedly inhibit the progression of pancreatic cancer, breast cancer, and nasopharyngeal carcinoma [12, 14]. We found that the active MPN domain of CSN5 was responsible for PD-L1 deubiquitination, and that an inhibitor of CSN5, C-15, inhibited tumor growth and the macrophage population and elevated cytotoxic T-cell activity by destabilizing PD-L1.

In summary, we revealed a molecular mechanism of immunosuppression in CRC cells—through CSN5-regulated PD-L1 stabilization, which was critical for the escape of cancer cells from immune surveillance. Importantly, C-15, an inhibitor of CSN5, significantly impaired PD-L1 stabilization in CRC cells, thus promoting the tumor-infiltrating cytotoxic T-cell response. Therefore, inhibition of PD-L1 stabilization in CRC cells by inactivating the CCL5-mediated p65/STAT3-CSN5-PD-L1 pathway shows therapeutic potential for CRC.

Data availability

The authors declare that all data supporting the finding of this study are available with the article or from the corresponding author upon reasonable request. The English in this document has been checked by at least two professional editors, both native speakers of English. For a certificate, please see: http://www.textcheck.com/certificate/a4R2bj

Acknowledgements This work was supported by the National Natural Science Foundation of China (Nos. 81702833, 81703781, 81803513, and 81803763), the Natural Science Foundation of Jiangsu Province (Nos. BK20170137 and BK20170140), Sichuan Science and Technology Program (No. 2018JY0204), Natural Science Foundation of Chengdu Medical College (No. CYZ17-13), Innovation of medical research youth in Sichuan (Grant No. Q17012), Jiangsu Provincial Special Program of Medical Science (BE2019617) and the Science and Technology Development Fund Project of Nanjing Medical University (No. 2016NJMUZD041, 2016NJMUZD043, and NMUB2018315). We thank the Cellular and Molecular Biology Center of China Pharmaceutical University for assistance with confocal microscopy work and we are grateful to Xiao-Nan Ma for her technical help.

Compliance with ethical standards

Conflict of interest The authors declare that they have no conflict of interest.

Publisher's note Springer Nature remains neutral with regard to jurisdictional claims in published maps and institutional affiliations.

References

1. Vinogradov S, Warren G, Wei X. Macrophages associated with tumors as potential targets and therapeutic intermediates. Nanomedicine. 2014;9:695–707.
2. Badawi MA, Abouelfadl DM, El-Sharkawy SL, El-Aal WEA, Abbas NF. Tumor-associated macrophage (TAM) and angiogenesis in human colon carcinoma. Open access Macedonian J Med Sci. 2015;3:209–14.
3. Bingle á, Brown N, Lewis C. The role of tumour-associated macrophages in tumour progression: implications for new anticancer therapies. J Pathol. 2002;196:254–65.
4. Zhang Q-w LiuL, Gong C-y ShiH-s, Zeng Y-h, Wang X-z, et al. Prognostic significance of tumor-associated macrophages in solid tumor: a meta-analysis of the literature. PLoS ONE. 2012;7:e50946.
5. Cai J, Qi Q, Qian X, Han J, Zhu X, Zhang Q, et al. The role of PD-1/PD-L1 axis and macrophage in the progression and treatment of cancer. J Cancer Res Clin Oncol. 2019;145:1377–85.
6. Mantovani A, Sozzani S, Locati M, Allavena P, Sica A. Macrophage polarization: tumor-associated macrophages as a paradigm for polarized M2 mononuclear phagocytes. Trends Immunol 2002;23:549–55.
7. Zhang S, Zhong M, Wang C, Xu Y, Gao WQ, Zhang Y. CCL5-deficiency enhances intratumoral infiltration of CD8(+) T cells in colorectal cancer. Cell Death Dis. 2018;9:766.

8. Chen J, Li G, Meng H, Fan Y, Song Y, Wang S, et al. Upregulation of B7-H1 expression is associated with macrophage infiltration in hepatocellular carcinomas. Cancer Immunol Immunother. 2012;61: 101–8.
9. Nijman SM, Luna-Vargas MP, Velds A, Brummelkamp TR, Dirac AM, Sixma TK, et al. A genomic and functional inventory of deubiquitinating enzymes. Cell. 2005;123:773–86.
10. Verma R, Aravind L, Oania R, McDonald WH, Yates JR, Koonin EV, et al. Role of Rpn11 metalloprotease in deubiquitination and degradation by the 26S proteasome. Science. 2002;298:611–5.
11. Ambroggio XI, Rees DC, Deshaies RJ. JAMM: a metalloprotease-like zinc site in the proteasome and signalosome. PLoS Biol. 2003;2:e2.
12. Pan Y, Yang H, Claret FX. Emerging roles of Jab1/CSN5 in DNA damage response, DNA repair, and cancer. Cancer Biol Ther. 2014;15:256–62.
13. Adler AS, Littlepage LE, Lin M, Kawahara TL, Wong DJ, Werb Z, et al. CSN5 isopeptidase activity links COP9 signalosome activation to breast cancer progression. Cancer Res. 2008;68:506–15.
14. Lim S-O, Li C-W, Xia W, Cha J-H, Chan L-C, Wu Y, et al. Deubiquitination and stabilization of PD-L1 by CSN5. Cancer Cell. 2016;30:925–39.
15. Watanabe K, Yokoyama S, Kaneto N, Hori T, Iwakami Y, Kato S, et al. COP9 signalosome subunit 5 regulates cancer metastasis by deubiquitinating SNAIL. Oncotarget. 2018;9:20670–80.
16. Du Q, Wang Q, Fan H, Wang J, Liu X, Wang H, et al. Dietary cholesterol promotes AOM-induced colorectal cancer through activating the NLRP3 inflammasome. Biochem Pharm. 2016;105:42–54.
17. Morrison DC, Ryan JL. Endotoxins and disease mechanisms. Annu Rev Med. 1987;38:417–32.
18. Meng F, Lowell CA. Lipopolysaccharide (LPS)-induced macrophage activation and signal transduction in the absence of Src-family kinases Hck, Fgr, and Lyn. J Exp Med. 1997;185:1661–70.
19. Hartley G, Regan D, Guth A, Dow S. Regulation of PD-L1 expression on murine tumor-associated monocytes and macrophages by locally produced TNF-α. Cancer Immunol Immunotherapy. 2017;66:523–35.
20. Wu Y, Deng J, Rychahou PG, Qiu S, Evers BM, Zhou BP. Stabilization of snail by NF-κB is required for inflammation-induced cell migration and invasion. Cancer Cell. 2009;15:416–28.
21. Sutterwala FS, Noel GJ, Salgame P, Mosser DM. Reversal of proinflammatory responses by ligating the macrophage Fcgamma receptor type I. J Exp Med. 1998;188:217–22.
22. Tang J, Qu LK, Zhang J, Wang W, Michaelson JS, Degenhardt YY, et al. Critical role for Daxx in regulating Mdm2. Nat Cell Biol. 2006;8:855–62.
23. Shackleford TJ, Zhang Q, Tian L, Vu TT, Korapati AL, Baumgartner AM, et al. Stat3 and CCAAT/enhancer binding protein beta (C/EBP-beta) regulate Jab1/CSN5 expression in mammary carcinoma cells. Breast Cancer Res. 2011;13:R65.
24. Kusaba T, Nakayama T, Yamazumi K, Yakata Y, Yoshizaki A, Nagayasu T, et al. Expression of p-STAT3 in human colorectal adenocarcinoma and adenoma; correlation with clinicopathological factors. J Clin Pathol. 2005;58:833–8.
25. Martinez Molina D, Jafari R, Ignatushchenko M, Seki T, Larsson EA, Dan C, et al. Monitoring drug target engagement in cells and tissues using the cellular thermal shift assay. Science. 2013;341:84–87.
26. Calderaro J, Rousseau B, Amaddeo G, Mercey M, Charpy C, Costentin C, et al. Programmed death ligand 1 expression in hepatocellular carcinoma: Relationship With clinical and pathological features. Hepatology. 2016;64:2038–46.
27. Wang X, Lang M, Zhao T, Feng X, Zheng C, Huang C, et al. Cancer-FOXP3 directly activated CCL5 to recruit FOXP3+Treg cells in pancreatic ductal adenocarcinoma. Oncogene. 2016;36: 3048.
28. Chen R, Lee WY, Zhang XH, Zhang JT, Lin S, Xu LL, et al. Epigenetic modification of the CCL5/CCR1/ERK axis enhances glioma targeting in dedifferentiation-reprogrammed BMSCs. Stem Cell Rep. 2017;8:743–57.
29. Zhou B, Sun C, Li N, Shan W, Lu H, Guo L, et al. Cisplatin-induced CCL5 secretion from CAFs promotes cisplatin-resistance in ovarian cancer via regulation of the STAT3 and PI3K/Akt signaling pathways. Int J Oncol. 2016;48:2087–97.
30. Huang CY, Fong YC, Lee CY, Chen MY, Tsai HC, Hsu HC, et al. CCL5 increases lung cancer migration via PI3K, Akt and NF-kappaB pathways. Biochem Pharmacol. 2009;77:794–803.
31. Zou W, Wolchok JD, Chen L. PD-L1 (B7-H1) and PD-1 pathway blockade for cancer therapy: Mechanisms, response biomarkers, and combinations. Sci Transl Med. 2016;8:328rv324.
32. Sun X-X, He X, Yin L, Komada M, Sears RC, Dai M-S. The nucleolar ubiquitin-specific protease USP36 deubiquitinates and stabilizes c-Myc. Proc Natl Acad Sci. 2015;112:3734.
33. Peth A, Berndt C, Henke W, Dubiel W. Downregulation of COP9 signalosome subunits differentially affects the CSN complex and target protein stability. BMC Biochem. 2007;8:27.
34. Dubiel D, Rockel B, Naumann M, Dubiel W. Diversity of COP9 signalosome structures and functional consequences. FEBS Lett. 2015;589:2507–13.
35. Zhu Y, Yang J, Xu D, Gao XM, Zhang Z, Hsu JL, et al. Disruption of tumour-associated macrophage trafficking by the osteopontin-induced colony-stimulating factor-1 signalling sensitises hepatocellular carcinoma to anti-PD-L1 blockade. Gut. 2019;68:1653–66.
36. Peranzoni E, Lemoine J, Vimeux L, Feuillet V, Barrin S, Kantari-Mimoun C, et al. Macrophages impede CD8 T cells from reaching tumor cells and limit the efficacy of anti–PD-1 treatment. Proc Natl Acad Sci. 2018;115:E4041.
37. Lee SJ, Jun SY, Lee IH, Kang BW, Park SY, Kim HJ, et al. CD274, LAG3, and IDO1 expressions in tumor-infiltrating immune cells as prognostic biomarker for patients with MSI-high colon cancer. J Cancer Res Clin Oncol. 2018;144:1005–14.
38. Kim JH, Park HE, Cho N-Y, Lee HS, Kang GH. Characterisation of PD-L1-positive subsets of microsatellite-unstable colorectal cancers. Br J Cancer. 2016;115:490.
39. Kather JN, Halama N, Jaeger D. Genomics and emerging biomarkers for immunotherapy of colorectal cancer. Semin Cancer Biol. 2018;52:189–97.
40. Häcker H, Karin M. Regulation and Function of IKK and IKK-Related Kinases. Sci STKE. 2006;2006:re13.
41. Lee H, Herrmann A, Deng J-H, Kujawski M, Niu G, Li Z, et al. Persistently activated Stat3 maintains constitutive NF-κB activity in tumors. Cancer Cell 2009;15:283–93.
42. Zhao R, Yeung SC, Chen J, Iwakuma T, Su CH, Chen B, et al. Subunit 6 of the COP9 signalosome promotes tumorigenesis in mice through stabilization of MDM2 and is upregulated in human cancers. J Clin Investig. 2011;121:851–65.
43. Schlierf A, Altmann E, Quancard J, Jefferson AB, Assenberg R, Renatus M, et al. Targeted inhibition of the COP9 signalosome for treatment of cancer. Nat Commun. 2016;7:13166.
44. Xiao D, Yang S, Huang L, He H, Pan H, He J. COP9 signalosome subunit CSN5, but not CSN6, is upregulated in lung adenocarcinoma and predicts poor prognosis. J Thorac Dis. 2018;10:1596–606.

Affiliations

Chao Liu[1,2] · Zhaoying Yao[1,2] · Jianing Wang[3] · Wen Zhang[1,2] · Yan Yang[4] · Yan Zhang[5] · Xinliang Qu[6] · Yubing Zhu[1,2] · Jianjun Zou[1,2] · Sishi Peng[2,7] · Yan Zhao[1,2] · Shuli Zhao[7] · Bangshun He[7] · Qiongyu Mi[7] · Xiuting Liu[8] · Xu Zhang[9,10,11] · Qianming Du[7]

1 Department of Pharmacy, Nanjing First Hospital, Nanjing Medical University, Nanjing 210006, PR China

2 Department of Clinical Pharmacy, School of Basic Medicine & Clinical Pharmacy, China Pharmaceutical University, Nanjing 210009, PR China

3 Neurobiology Laboratory, Jiangsu Center for Drug Screening, China Pharmaceutical University, Nanjing 210009, PR China

4 Department of Pharmacy, The Third People's Hospital of Chengdu & Affiliated Hospital of Southwest Jiaotong University, 82 Qing Long Street, Chengdu 610031, PR China

5 Department of Gastroenterology, Nanjing First Hospital, Nanjing Medical University, Nanjing 210006, PR China

6 Department of Cardiology, Nanjing First Hospital, Nanjing Medical University, Nanjing 210006, PR China

7 General Clinical Research Center, Nanjing First Hospital, Nanjing Medical University, Nanjing 210006, PR China

8 Department of Medicine, Washington University School of Medicine, St. Louis, MO 63110, USA

9 Department of Pharmacy, The First People's Hospital of Chengdu & Affiliated Hospital of Chengdu Medical College, 18 Wanxiang East Road, Chengdu 610041, PR China

10 Affiliated Hospital of integrated traditional Chinese and Western Medicine of Chengdu Medical College, 783 Xindu Avenue, Chengdu 610031, PR China

11 Affiliated Hospital of integrated traditional Chinese and Western Medicine of Chengdu University of TCM, 37, Twelve Bridges Road, Chengdu 610031, PR China